PAPER Special Section on Medical Information Communication Technology for Disaster Recovery and Human Health Care Support

Performance Evaluation on RSSI-Based Localization for Capsule Endoscopy Systems with 400 MHz MICS Band Signals

Daisuke ANZAI[†a)], ***Member***, **Sho AOYAMA**[†], ***Student Member***, ***and*** **Jianqing WANG**[†b)], ***Fellow***

SUMMARY One of promising application offered by implant body area networks (BANs) is a capsule endoscope localization system. To begin with, this paper performs finite-difference time-domain (FDTD) simulations on implant BAN propagation with a numerical human model, and investigates the propagation characteristics of implant BAN signals at 400 MHz medical implant communication service (MICS) band. Then, the paper presents a capsule endoscope localization system which utilizes only received signal strength indicator (RSSI) and two estimation methods, such as a maximum likelihood (ML) estimation method and a least squares (LS) method. Furthermore, we evaluate the two localization methods by two computer simulation scenarios. Our computer simulation results demonstrate that the ML localization can improve the location estimation accuracy as compared with the LS localization, that is, our performance comparison reveals that a careful consideration the propagation characteristics of implant BANs signals is efficient in terms of estimation performance improvement in capsule endoscope localization.

key words: *implant BANs, localization, RSSI*

1. Introduction

Body area networks (BANs) have drawn considerable attention in healthcare and medical applications with the rapid growth of small devices and wireless communications [1]–[3]. BANs are generally categorized into two groups, namely, wearable BANs and implant BANs. One of applications by using wearable BANs is medical monitoring, which can be used to monitor a person's healthy situation in daily life [2]. On the other hand, in implant BANs, capsule endoscopy has been one of the most important applications [4], [5]. Capsule endoscopy involves ingesting a small capsule, which contains a color camera, battery, light source and transmitter. The capsule endoscope takes pictures every second and transmits images to a data recorder in order to assist in diagnosing gastrointestinal conditions such as obscure gastrointestinal bleeding, malabsorption, chronic abdominal pain and chronic diarrhoea. In this paper, we pay attention to the capsule endoscopy system, namely, implant BAN applications.

Since a capsule endoscope moves inside a human body, nobody knows the location of the capsule endoscope in advance. Moreover, the location information of the capsule endoscope makes it easier to detect diagnose gastrointestinal conditions. Therefore, in the capsule endoscopy systems, it is important to estimate and track the capsule endoscope location. Generally, localization methods are based on measuring the distances between transceivers. Time of arrival (TOA)-, time difference of arrival (TDOA)-, angle of arrival (AOA)-based methods show better location accuracy, however, they require precise synchronization among the local oscillators of wireless nodes, several types of signals with different velocities and multiple antennas at nodes, respectively [6]–[8]. Therefore, they are disadvantageous in terms of cost and energy consumption of transceivers.

On the other hand, received signal strength indicator (RSSI)-based location estimation method is advantageous in terms of cost and energy consumption, because most of the current wireless communication standards, such as the IEEE 802.11 standard, IEEE 802.15.4 standard and so on, have a function of measuring RSSI in their protocols [9]. However, the RSSI-based location estimation shows poor accuracy in real environments because multipath fading gives large variations to measured RSSIs, that is, the estimation performance depends much on the propagation characteristics of implant BAN signals. Therefore, in order to improve the performance of RSSI-based location estimation, a maximum likelihood (ML) method has been so far proposed [10], [11]. Furthermore, it is reported that an RSSI-based ML localization method outperforms a TDOA-based method when the direct link between transceivers are often shadowed [12].

However, to use an ML estimation method, a statistical model on the RSSI is required in advance, which can well characterize the real variation of the RSSI in the location estimation area. So, in order to successfully apply an ML estimation technique to capsule endoscope localization, we should derive a statistical model of the propagation characteristics of implant BANs signals. In this paper, we pay attention to 400 MHz medical implant communication service (MICS) band. As related works, several papers have so far investigated the propagation characteristics and proposed path loss models for the capsule endoscopy [13], [14]. However, to the best of the authors' knowledge, there is no investigation for the purpose of the propagation characteristics for ML localization in the implant BANs, therefore, in this paper, we investigate the propagation characteristics by using finite-difference time-domain (FDTD) simulations. In place of the difficulty in actual measurement of propagation characteristics for living humans, FDTD simulation has a merit to provide high-quality propagation data by using an anatomically based high-resolution human body model

Manuscript received January 16, 2012.
Manuscript revised May 1, 2012.

[†]The authors are with Nagoya Institute of Technology, Nagoya-shi, 466-8555 Japan.
a) E-mail: anzai@nitech.ac.jp
b) E-mail: wang@nitech.ac.jp

DOI: 10.1587/transcom.E95.B.3081

[15].

In this paper, to begin with, we present the propagation characteristics of the 400 MHz MICS band signals which are obtained by FDTD simulations. Based on the FDTD-simulated data, the paper then constructs a statistical model on the propagation characteristics, and presents a capsule endoscopy localization systems. Here, in addition to the ML localization, we take least squares (LS) localization into consideration as a comparison method, which considers only an average path loss effect. Finally, we evaluate the performances of the ML localization and the LS localization by computer simulations with two scenarios, and discuss the estimation accuracies of the two localization methods in the capsule endoscopy systems.

2. Propagation Characteristics

We investigate the propagation characteristics by using a FDTD simulation. The FDTD simulation uses a numerical human model developed by National Institute of Information and Communication Technology (NICT), Japan [16]–[18]. This model is segmented into 51 different tissues and organs, and the masses of main tissues and organs are compared with the average values for Japanese reference man. The height and the weight of the numerical human model are 1.73 m and 65 kg, respectively, and the voxel size of the FDTD simulation is 4 mm × 4 mm × 4 mm. In a similar way of the system model, a transmitter locates inside of the human body and receivers are put on the human body. In the FDTD simulation, we put the transmitter on 30 points inside the human body, such as the esophagus, stomach, small intestine and large intestine. In order to analyze the electromagnetic field of the FDTD simulation environment, the space step size must be much smaller than the wavelength of the transmitted signal. The frequency band of the transmitted signal f_c is 400 MHz band, so the voxel size of 4 mm is enough smaller than the wavelength even if the transmitted signal propagates through the human tissues. Furthermore, based on the Courant stability condition, we set the time step to 7.70 psec. On the other hand, we put 14 receivers on the human body, which employs dipole antennas with the length of 20 mm. For the purpose of simplification of the receivers placement and their locations measurement, they are located around the chest and the abdomen as shown in Fig. 1.

According to an empirical power decay law, the average path loss $PL_{dB}^{average}$ is expressed as

$$PL_{dB}^{average} = PL_{0,dB} + 10\log_{10}\left(\frac{d}{d_0}\right)^n \tag{1}$$

where d, $PL_{0,dB}$ and n denote the distance between the transmitter and the receiver, the reference path loss at the distance d_0, the path loss exponent, respectively. Here, we define the path loss PL_{dB} as

$$PL_{dB} = 10\log_{10}\frac{P_t}{P_r} + G_{t,dB} + G_{r,dB} \tag{2}$$

where P_t, P_r, $G_{t,dB}$ and $G_{r,dB}$ denote the transmitted power, the received power (RSSI in this paper), the transmit antenna gain and the receive antenna gain in unit of dB, respectively. From (1) and (2), the average received power $\overline{P_r}$ is given by

$$\overline{P_r} = \alpha d^{-n} \tag{3}$$

where α is a constant coefficient which is uniquely determined by the propagation environment. Figure 2 shows a power decay characteristic, namely, the $\overline{P}$ against the distance d for all the receivers. Figure 2 also includes a fitted curve given by Eq. (3) whose parameters are estimated by a least squares method. From this figure, the average received power is proportional to d^n. Because the correlation coefficient between the FDTD-simulated data and the data obtained by the fitted curve is 0.985, we can see that the average received power $\overline{P}$ is well approximated by Eq. (3).

Next, we consider a shadowing effect, namely, a shadow fading characteristic in the implant BAN channels. We define the path loss S_{dB} normalized by Eq. (1) as

$$S_{dB} = PL_{dB}^{instant} - PL_{dB}^{average} \tag{4}$$

where $PL_{dB}^{instant}$ is the instant path loss. Figure 3 shows the cumulative distribution function (*cdf*) against the normalized path loss S_{dB} at the all receivers. Furthermore, Fig. 3

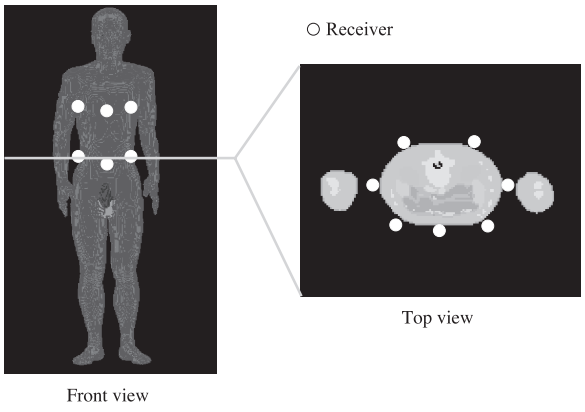

Fig. 1 Receivers deployment on numerical human model.

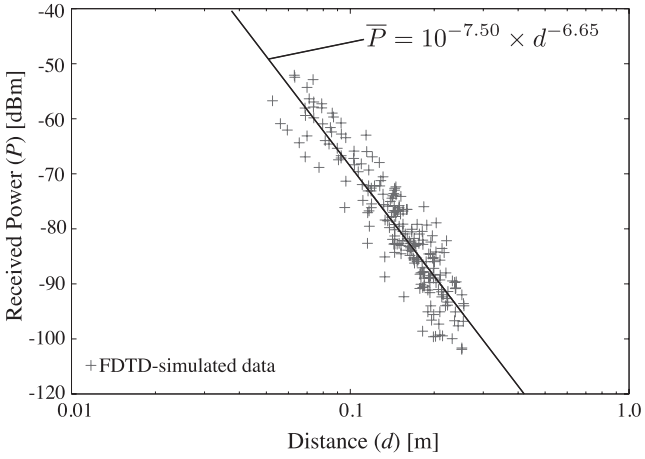

Fig. 2 Power decay characteristic.

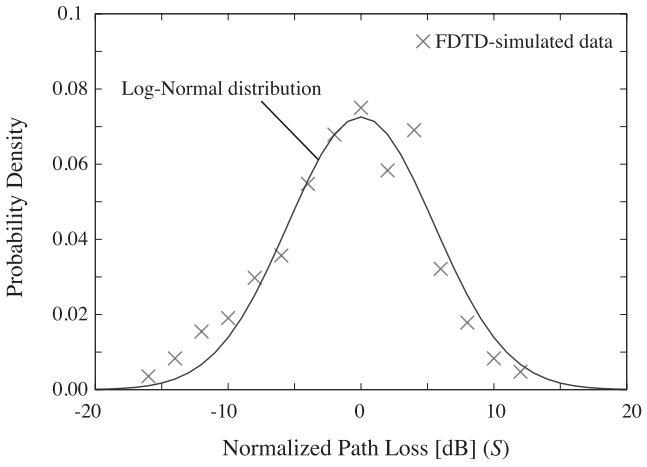

Fig. 3 Shadow fading characteristic.

also shows the Log-Normal distribution given by

$$p(S) = \frac{1}{\sqrt{2\pi}\sigma S} \exp\left[-\frac{(\log S - \mu)^2}{2\sigma^2}\right]. \quad (5)$$

In (5), σ and μ represent the standard deviation and the average in log domain, respectively, and in Fig. 3, these parameters are calculated by a least squares method. From the figure, the shadowing effect is well approximated by the Log-Normal distribution with the correlation coefficient of 0.935.

Finally, from all the FDTD-simulated results, we have come to a conclusion that the variation of the RSSIs can be well modeled with the following two-layered model:

$$p(P_r|d) = \frac{1}{\sqrt{2\pi}\sigma P_r} \exp\left[-\frac{\{\log P_r - \mu(d)\}^2}{2\sigma^2}\right] \quad (6)$$

$$\mu(d) = \log \overline{P_r} = \log[\alpha d^{-n}]. \quad (7)$$

In reality, even in the FDTD simulation, each receiver at a different location has a different channel parameter. However, taking a realistic solution for capsule endoscope localization into consideration, it is difficult to measure channel model parameters for different receiver locations because the total number of channel model parameters increases with the number of receivers. So, in this paper, the above two-layered model assumes an average field on the propagation characteristics (a single channel model parameter).

3. System Model for Capsule Endoscope Localization

We assume a capsule endoscope (transmitter) inside a human body and L receivers on the human body as shown in Fig. 1. The capsule endoscope location is unknown and the L receiver locations are known in advance, so the capsule endoscope location should be estimated with information of the L receiver locations. We define the locations of the capsule endoscope and the l-th receiver ($l = 1, \cdots, L$) in column vector forms (3×1) respectively as

$$\mathbf{t} = [x, y, z]^T \quad (8)$$

$$\mathbf{r}_l = [x_l, y_l, z_l]^T \quad (9)$$

where x, y and z are the unknown coordinates of the capsule endoscope location, respectively, x_l, y_l and z_l are the known coordinates of the l-th receiver location, respectively, and T denotes transpose.

In the localization system, the capsule endoscope transmits M packets to receivers and the receivers measures an RSSI for each received packet. The location of the capsule endoscope is finally estimated according to a location estimation method in a centralized manner.

4. Localization Principle

4.1 ML Localization

Define the distance between the capsule endoscope and the l-th receiver and the RSSI vector ($L \times 1$) for the m-th packet ($m = 1, \cdots, M$) respectively as

$$d_l(\mathbf{t}) = |\mathbf{t} - \mathbf{r_l}| = \sqrt{(x - x_l)^2 + (y - y_l)^2 + (z - z_l)^2} \quad (10)$$

$$\mathbf{P}_m = [P_{1m}, \cdots, P_{Lm}]^T \quad (11)$$

where P_{lm} denotes the RSSI of the m-th packet transmitted from the capsule endoscope and then measured at the l-th receiver. The log-likelihood function on $\mathbf{t}$ is written as

$$L(\mathbf{t}) = \log p(\mathbf{P}_1, \mathbf{P}_2, \cdots, \mathbf{P}_M|\mathbf{t}). \quad (12)$$

Assume that P_{nm} is independent of $P_{lm'}$ ($m \neq m'$) (*temporal whiteness*) and $P_{l'm}$ ($l \neq l'$) (*geographical whiteness*). In this case, replacing d by $d_l(t)$ and P_r by P_{lm} respectively in (6) and (7) (also $\overline{P_r}$ by $\overline{P_l}$), (12) results in

$$L(\mathbf{t}) = \log\left[\prod_{m=1}^{M}\prod_{l=1}^{L} p(P_{lm}|d_l(\mathbf{t}))\right] = \sum_{m=1}^{M}\sum_{l=1}^{L}\left[-\log\sqrt{2\pi}\sigma P_{lm} - \frac{(\log P_{lm} - \mu[d_l(\mathbf{t})])^2}{2\sigma^2}\right]. \quad (13)$$

Now, the ML estimation gives the estimated location of the capsule endoscope $\hat{\mathbf{t}}_{ML}$ which maximizes (13), so $\hat{\mathbf{t}}_{ML}$ can be obtained from the following maximum likelihood equation:

$$\left.\frac{\partial L(\mathbf{t})}{\partial \mathbf{t}}\right|_{\mathbf{t}=\hat{\mathbf{t}}_{ML}} = 0. \quad (14)$$

4.2 LS Localization

In addition to the ML localization, we take LS localization into consideration. Defining the m-th estimate of distance between the l-th receiver and the capsule endoscope as $\hat{d}_{lm}$,

Table 1 Computer simulation scenarios.

	Ideal environment (Scenario A)	Realistic environment (Scenario B)
Shape of location estimation area	Cube	Human body
RSSI generation	Random number generation based on (6) with parameters of $\alpha = 10^{-7.50}$, $n = 6.65$ and $\sigma = 5.50$	FDTD simulation
Number of receivers (L)	8	14

the location of the capsule endoscope is calculated by minimizing the sum of the estimation errors as

$$\text{find } x, y, z \text{ which minimizes } e \tag{15}$$

$$e = \sum_{m=1}^{M} \sum_{l=1}^{L} \left| \hat{d}_{lm} - \sqrt{(x-x_l)^2 + (y-y_l)^2 + (z-z_l)^2} \right| \tag{16}$$

where

$$\hat{d}_{lm} = \left(\frac{P_{lm}}{\alpha} \right)^{-1/n}. \tag{17}$$

Note that the LS localization considers only the average path loss effect, in other words, it does not take account of the instantaneous RSSI variation represented by (6). On the other hand, the ML localization considers not only the average path loss effect but also the instantaneous RSSI variation expressed as (6) and (7).

4.3 Cramer-Rao Lower Bound Analysis

The quality of the estimate of $\mathbf{t}$ can be measured in terms of the variance. The Cramer-Rao lower bound (CRLB) [19] provides a lower bound on the minimum error variance for the ML estimation. When the elements of $\mathbf{t}$ are treated as uniform random variables, the CRLB is given by the diagonal elements of the inverse of the information matrix $\mathbf{J}_F$, which denotes the Fisher information matrix representing the information obtained from the measurements. Here, $\mathbf{J}_F$ is written as

$$\mathbf{J}_F = -E\left\{ \left[\frac{\partial}{\partial \mathbf{t}} L(\mathbf{t}) \right] \left[\frac{\partial}{\partial \mathbf{t}} L(\mathbf{t}) \right]^T \right\}. \tag{18}$$

Let $\mathbf{I}$ and I_{ii} denote the inverse matrix of $\mathbf{J}_F$ and its i-th diagonal element, respectively. In this case, the minimum location error variance for the ML estimation σ^2_{CRLB} is given by

$$\begin{aligned} \sigma^2_{CRLB} &= \min(var[x] + var[y] + var[z]) \\ &= I_{11} + I_{22} + I_{33}. \end{aligned} \tag{19}$$

5. Performance Evaluation

5.1 Computer Simulation Scenarios

To evaluate the performance of the localization methods, we conducted computer simulations. In the computer simulations, this paper considers two simulation scenarios. One is a computer simulation in an ideal environment (Scenario A), where measured RSSI is generated as a random variable whose pdf is given by (6), namely, the variation of RSSI is perfectly corresponding to the propagation model described by (6) and (7). On the other hand, the other is a computer simulation in a realistic environment (Scenario B). In this scenario, measured RSSI is calculated by the FDTD simulations with the numerical human model described in Sect. 2. In place of the difficulty in actual measurement of propagation characteristics for living humans, FDTD simulation has a merit to provide high-quality propagation data, namely, RSSI variations in realistic implant BANs, by using an anatomically based high-resolution human body model [15]. Therefore, in this sense, as compared with the case of Scenario A, the computer simulation with Scenario B can better demonstrate the performance in a realistic environment. Table 1 summarizes the two computer simulation scenarios.

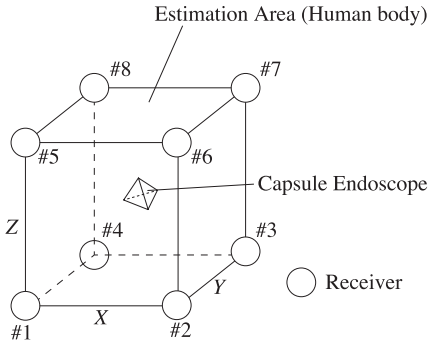

Fig. 4 Location estimation area. (Scenario A)

5.2 Computer Simulation in Ideal Environment (Scenario A)

In this computer simulation scenario, we assumed a cuboid location estimation area shown in Fig. 4, whose size was $X = 0.4\,\text{m}$ (width) $\times$ $Y = 0.2\,\text{m}$ (depth) $\times$ $Z = 0.4\,\text{m}$ (height). As shown in Fig. 4, we used 8 receivers and put them at each vertex of the cubic location estimation area. The locations of the capsule endoscope were randomly chosen at 5000 points. The channel model parameters α, n and σ were determined by the FDTD-simulated data as $\alpha = 10^{-7.50}$, $n = 6.65$ and $\sigma = 5.50$.

Figure 5 shows the root mean square (RMS) location estimation error (namely, the standard deviation of the location estimation error) with respect to the number of transmitted packets M for the ML localization and the LS localization. Furthermore, Fig. 5 also includes the theoret-

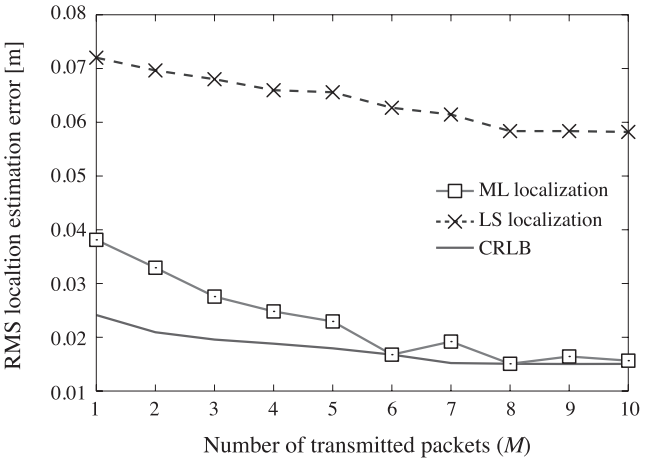

Fig. 5 Performance comparison of ML localization and LS localization. (Scenario A)

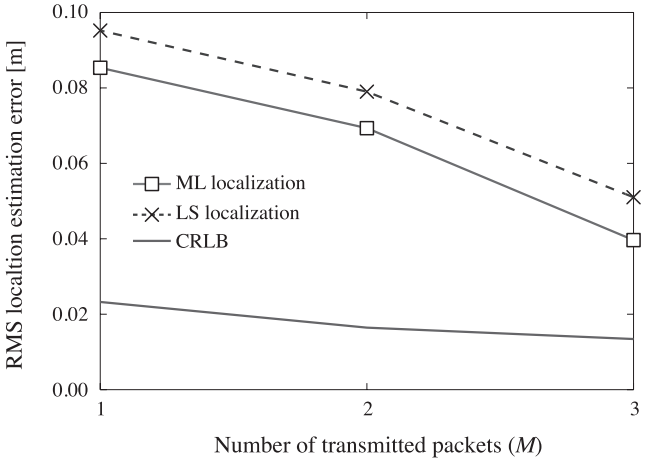

Fig. 7 Performance comparison of ML localization and LS localization. (Scenario B)

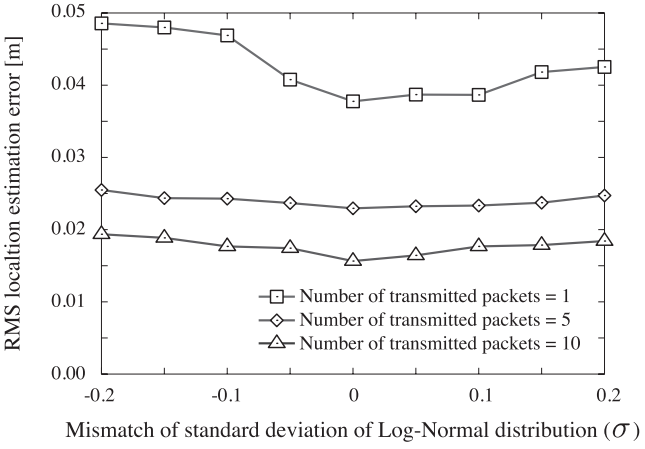

Fig. 6 Mismatch of standard deviation of Log-Normal distribution for ML localization. (Scenario A)

ical bounds, namely, the CRLB for the ML localization. Here, we assume that the channel parameters α, n and σ are perfectly estimated in advance. From this figure, as the number of transmitted packets increases, the location estimation error gradually decreases because more transmitted packets (RSSI information) can be used for location estimation. Moreover, the performance of the ML localization converges to the CRLB, so the efficiency of the ML estimator can be established. We can also see from the computer simulation result that the performance of the ML localization is better than that of the LS localization. Therefore, the use of the statistical model on the RSSI variation represented by (6) can improve the estimation accuracy. For example, at the number of transmitted packets = 10, as compared with the LS localization, the ML localization improves the performance by 80%.

In the ML localization, additional information of the channel parameter σ is required to solve the maximum likelihood equation represented by (14). So, in Fig. 5, we have so far assumed that the channel parameters are perfectly estimated in advance. On the other hand, Fig. 6 shows the RMS estimation error for the ML localization against the mismatch of the channel parameter, i.e., the standard deviation of the Log-Normal distribution σ. There are three curves in this figure, corresponding to the performance with the number of transmitted packets=1, 5 and 10, respectively. If the channel parameter is accurately estimated, the ML localization system with more RSSI information gives better estimation performance, whereas it cannot always give an accurate estimate of the capsule endoscope location with an inaccurate estimated channel parameter. Hence, accurate pre-estimation of the channel parameter is essential for a given location estimation area where we want to conduct capsule endoscope location estimation. However, a joint ML location/channel parameters estimation method has been proposed in [11], and therefore, if the joint estimation technique can be applicable to the ML localization, it might not require pre-estimation of the channel parameters without loss of the location estimation accuracy.

5.3 Computer Simulation in Realistic Environment (Scenario B)

In addition to the computer simulation in the ideal environment (Scenario A), we also conducted another computer simulation in a more realistic environment (Scenario B). In this computer simulation scenario, RSSIs were calculated based on FDTD simulation with the numerical human model used in Sect. 2. We put 14 receivers on the numerical human model as shown in Fig. 1, and a transmitter was located at 30 locations selected in the apparatus digestorius of the human body (4 locations in esophagus, 4 locations in stomach, 9 locations in small intestine and 13 locations in large intestine). We set the direction of transmit antenna randomly chosen from X-axis, Y-axis and Z-axis. As a result, the maximum number of transmitted packets is 3 because the transmit antenna may take three directions at a location.

Figure 7 shows the RMS location estimation error with

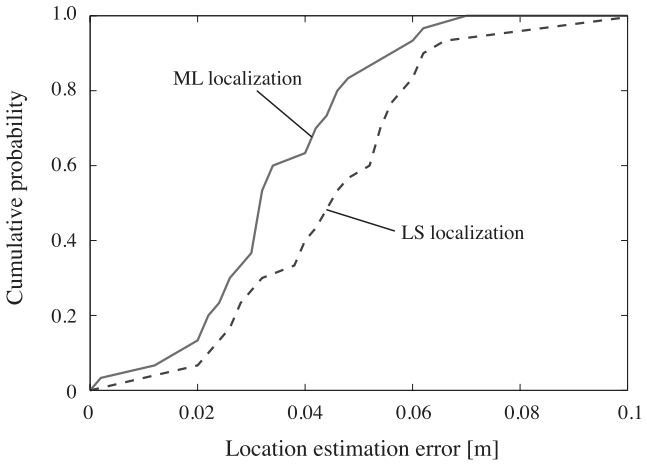

Fig. 8 Cumulative probability of location estimation error. (Scenario B)

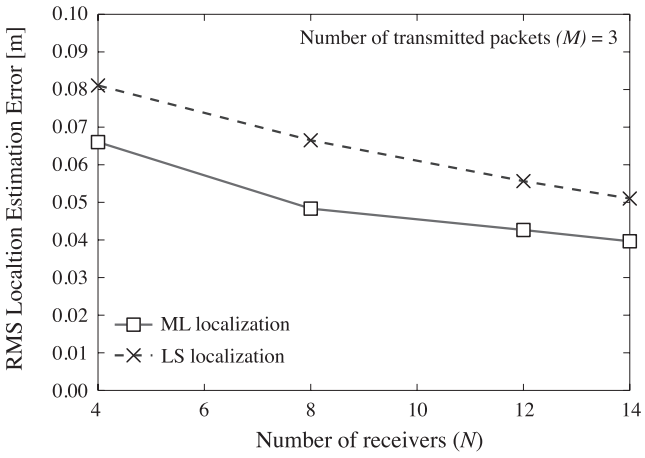

Fig. 9 Impact of the number of receivers on location estimation error. (Scenario B)

respect to the number of transmitted packets M for the ML localization and the LS localization. From this figure, similarly to the result of Scenario A, as the number of transmitted packets increases, the location estimation error gradually decreases. Moreover, the ML localization is superior to the LS localization in terms of the estimation accuracy in not only Scenario A but also Scenario B. Therefore, the use of the statistical model on the RSSI variation represented by (6) can also improve the estimation accuracy. In our evaluation based on the FDTD simulation, at the number of transmitted packets = 3, the estimation accuracies of 4 cm and 5 cm are accomplished by the ML localization and the LS localization, respectively.

Then, we discuss the estimation accuracy of the RSSI-based localization. In [20], the RSSI-based ranging (namely, 1-demensional localization) was evaluated, and the average error resulted in 0.037 m. Therefore, taking into consideration that our localization estimates the 3-demensional location, the estimation accuracy of around 0.04 m obtained by our computer simulation might be better than the result in [20]. Furthermore, the CRLB indicates the possibility of more accurate RSSI-based localization, e.g. at the number of transmitted packets of 3, the CRLB of 0.01 m can be achieved.

Figure 8 shows the cumulative probability of the location estimation errors for the ML localization and the LS localization. We can see from the figure that the ML localization can also improve the performance from the viewpoint of the cumulative probability as well as the RMS location estimation error. For example, with the cumulative probability of 0.8, the location estimation performance for the ML localization can be improved by about 35%, as compared with that for the LS localization. Furthermore, from this result, we can see that the maximum errors of the ML localization and LS localization are 0.07 m and 0.1 m, respectively. Note that the maximum errors of the ML and LS localization have occurred in the small intestine.

Finally, Fig. 9 shows the RMS location estimation error versus the number of the receivers N. This result demonstrates that the location estimation performance is improved with increasing the number of the receivers. As a result, it is significant to increase not only the number of transmitted packets but also the number of the receivers in terms of the improvement of the estimation accuracy.

6. Conclusions

To derive a statistical model on RSSIs for capsule endoscope localization in implant BANs, we have performed FDTD simulations with a numerical human model, and investigated the propagation characteristics of implant BAN signals at MICS 400 band. Then, this paper has presented a capsule endoscope localization system with two localization methods, such as the ML estimation method and the LS estimation method, and evaluated the estimation accuracy by the computer simulations with the two scenarios. The results of Scenario A have demonstrated that the performance of the ML localization can be improved by around 80% as compared with the LS localization. Furthermore, as the number of the transmitted packets increases, the performance of the ML localization converges to the CRLB. On the other hand, from the results of Scenario B, we have confirmed that the achievable RMS location estimation errors for the ML localization and the LS localization are 4 cm and 5 cm, respectively. The reason why the ML localization outperforms the LS localization is that the ML localization considers the both effects, namely, the average path loss by (6) and the instantaneous RSSI variation by (7), whereas the LS localization considers only the average path loss effect. Consequently, our performance comparison with the both scenarios can conclude that a careful consideration of the propagation characteristics of implant BANs signals is important in terms of estimation performance improvement in capsule endoscope localization.

Several papers have so far proposed capsule endoscope localization methods based on other techniques, e.g. TOA technique [6]. Our future subject is to investigate its feasibility in three–dimensional estimation accuracy and com-

pare the performances between RSSI-based localization and other localization in the same simulation environment, including investigation of the channel model parameters and the estimation accuracy in another numerical human model.

Acknowledgment

This study was supported in part by a Grant-in-Aid for Young Scientists (B) (No. 24760297) from the Ministry of Education, Science, Sport and Culture of Japan.

References

[1] H.B. Li and R. Kohno, "Body area network and its standardization at IEEE 802.15. BAN," Advances in Mobile and Wireless Communications, pp.223–238, Springer, 2008.
[2] E. Monton, J.F. Hernandez, J.M. Blasco, T. Herve, J. Micallef, I. Grech, A. Brincat, and V. Traver, "Body area network for wireless patient monitoring," IET Commun., vol.2, no.2, pp.215–222, Feb. 2008.
[3] V. Leonov, P. Fiorini, S. Sedky, T. Torfs, and C. Van Hoof, "Thermoelectric MEMS generators as a power supply for a body area network," Proc. IEEE Solid-State Sensors, Actuators and Microsystems 2005, vol.1, pp.291–294, June 2005.
[4] G. Iddan, G. Meron, A. Glukhovsky, and P. Swain, "Wireless capsule endoscopy," Nature, vol.405, p.417, May 2000.
[5] G. Costamagna, S.K. Shah, M.E. Riccioni, F. Foschia, M. Mutignani, V. Perri, A. Vecchioli, M.G. Brizi, A. Picciocchi, and P. Marano, "A prospective trial comparing small bowel radiographs and video capsule endoscopy for suspected small bowel disease," Gastroenterology, vol.123, no.4, pp.999–1005, Oct. 2002.
[6] M. Kawasaki and R. Kohno, "Position estimation method of medical implanted devices using estimation of propagation velocity inside human body," IEICE Trans. Commun., vol.E92-B, no.2, pp.403–409, Feb. 2009.
[7] N.B. Priyantha, A. Chakraborty, and H. Balakrishnan, "The cricket location-support system," Proc. ACM MOBICOM, pp.112–121, Aug. 2000.
[8] D. Niculescu and B. Nath, "Ad hoc positioning system (APS) using AOA," Proc. IEEE INFOCOM 2003, vol.3, pp.1734–1743, April 2003.
[9] A. Hac, Wireless Sensor Network Designs, Wiley, 2003.
[10] D. Anzai and S. Hara, "A simple outlier data rejection algorithm for an RSSI-based ML location estimation in wireless sensor networks," Proc. IEEE VTC 2008-Fall, pp.1–5, Sept. 2008.
[11] R. Zemek, D. Anzai, S. Hara, K. Yanagihara, and K. Kitayama, "RSSI-based localization without a prior knowledge of channel model parameters," Int. J. Wireless Information Networks, vol.15, no.3–4, pp.128–136, Oct. 2008.
[12] S. Hara and D. Anzai, "Experimental performance comparison of RSSI- and TDOA-based location estimation methods," Proc. IEEE VTC 2008-Spring, pp.2651–2655, May 2008.
[13] T. Aoyagi, K. Takizawa, T. Kobayashi, J. Takada, K. Hamaguchi, and R. Kohno, "Development of an implantable WBAN path-loss model for capsule endoscopy," IEICE Trans. Commun., vol.E93-B, no.4, pp.846–849, April 2010.
[14] K. Sayrafian-Pour, W. Yang, J. Hagedorn, J. Terrill, and K.Y. Yazdandoost, "A statistical path loss model for medical implant communication channels," Proc. IEEE PIMRC 2009, pp.2995–2999, Sept. 2009.
[15] J. Wang, Y. Nishikawa, and T. Shibata, "Analysis of on-body transmission mechanism and characteristic based on an electromagnetic field approach," IEEE Trans. Microw. Theory Tech., vol.57, no.10, pp.2464–2470, Oct. 2009.
[16] T. Nagaoka, S. Watanabe, K. Sakurai, E. Kunieda, S. Watanabe, M. Taki, and Y. Yamanaka, "Development of realistic high-resolution whole-body voxel models of Japanese adult males and females of average height and weight, and application of models to radio-frequency electromagnetic-field dosimetry," Phys. Med. Biol., vol.49, pp.1–15, Jan. 2004.
[17] J. Wang, O. Fujiwara, S. Kodera, and S. Watanabe, "FDTD calculation of whole-body average SAR in adult and child models for frequencies from 30 MHz to 3 GHz," Phys. Med. Biol., vol.51, no.17, pp.4119–4127, Aug. 2006.
[18] J. Wiart, A Hadjem, M.F. Wong, and I. Bloch, "Analysis of RF exposure in the head tissues of children and adults," Phys. Med. Biol., vol.53, no.13, pp.3681–3695, June 2008.
[19] H.L. Van Trees, Detection, Estimation, and Modulation Theory: Part I, Wiley, 1968.
[20] L. Lin, M. Rasouli, A.P. Kencana, S.L. Tan, K.J. Wong, K.Y. Ho, and S.J. Phee, "Capsule endoscopy — A mechatronics perspective," Frontiers of Mechanical Engineering, vol.6, no.1, pp.33–39, 2011.

Daisuke Anzai received the B.E., M.E. and Ph.D. degrees from Osaka City University, Osaka, Japan in 2006, 2008 and 2011, respectively. Since April 2011, he has been an Assistant Professor at the Graduate School of Engineering, Nagoya Institute of Technology, Nagoya, Japan. He has engaged in the research of biomedical communication systems and localization systems in wireless communication networks.

Sho Aoyama was born in Aichi, Japan, in 1989. He received the B.Eng. degree from Nagoya Institute of Technology, Aichi, Japan in 2011. He is currently pursuing the M.Eng. course at Nagoya Institute of Technology, engaging in the research on wireless communication in body area networks.

Jianqing Wang received the B.E. degree in electronic engineering from Beijing Institute of Technology, Beijing, China, in 1984, and the M.E. and D.E. degrees in electrical and communication engineering from Tohoku University, Sendai, Japan, in 1988 and 1991, respectively. He was a Research Associate at Tohoku University and a Senior Engineer at Sophia Systems Co., Ltd., prior to joining the Nagoya Institute of Technology, Nagoya, Japan, in 1997, where he is currently a Professor. His research interests include biomedical communications and electromagnetic compatibility.